Cryogenics 126 (2022) 103535

Contents lists available at ScienceDirect

Cryogenics

journal homepage: www.elsevier.com/locate/cryogenics

Design and optimization of the four-stage recuperative coiled tube-in-tube heat exchanger for a 1.8 K hybrid cryocooler

Bangjian Zhao [a,c], Tao Zhang [a,c], Jun Tan [a], Yongjiang Zhao [a,c], Renjun Xue [a,c], Han Tan [a,c], Shiguang Wu [a,c], Yujia Zhai [a,c], Haizheng Dang [a,b,c,d,*]

[a] State Key Laboratory of Infrared Physics, Shanghai Institute of Technical Physics, Chinese Academy of Sciences, 500 Yutian Road, Shanghai 200083, China
[b] Shanghai Research Center for Quantum Sciences, Shanghai 201315, China
[c] University of Chinese Academy of Sciences, No.19A Yuquan Road, Beijing 100049, China
[d] Shanghai Boreas Cryogenics Co., Ltd, Shanghai 201802, China

ARTICLE INFO

Keywords:
Recuperative coiled tube-in-tube heat exchanger
4–300 K
Design and optimization
Heat exchanger effectiveness
Pressure drop
1.8 K hybrid cryocooler

ABSTRACT

The recuperative coiled tube-in-tube heat exchanger (RCTTHE) is a key component of the hybrid cryocooler formed by a four-stage Stirling-type pulse tube cryocooler and a JT cooler, and its heat exchanger effectiveness and pressure drop of low-pressure side play an important role in enhancing the overall performance of the hybrid cryocooler. This paper develops a finite difference model to systematically investigate the four-stage RCTTHE. The flow and heat transfer characteristics in the temperature range of 4–300 K under different dimensional and operating parameters are investigated in detail. The heat exchanger effectiveness and pressure drop of the low-pressure side are optimized to meet the requirements of the 1.8 K hybrid cryocooler with He-4 as the only working medium. The experimental investigations of the hybrid cryocooler based on the optimized four-stage RCTTHE are conducted. Satisfactory agreements are observed between the theoretical and experimental data, and thus verify the proposed model. The experimental results show that the pressure drop of the low-pressure side of the RCTTHE reaches a considerably low value of 518 Pa and an effectiveness of higher than 97.1 % is achieved for the four-stage RCTTHE, both of which make a significant contribution to the hybrid cryocooler in achieving 1.8 K.

1. Introduction

With the rapid progress of the deep space exploration and quantum information technology, there is an increasing demand for the cryocoolers operating at below 2 K which features high reliability, long lifetime, lightweight and high thermodynamic effectiveness [1–8]. The hybrid cryocooler formed by the multi-stage Stirling-type pulse tube cryocooler (SPTC) and the Joule-Thomson cooler (JTC) was an enabling technology to meet the requirements [5–7]. We recently reported a hybrid cryocooler composed of a four-stage SPTC and a JTC developed in the authors' laboratory [9–11], which reached a no-load temperature of 1.36 K with He-4 in the SPTC and He-3 in the JTC, respectively [11]. Considering He-3 was rare and expensive [12], we further improved the hybrid cryocooler with He-4 as the only working medium in the entire system and recently achieved a no-load temperature of 1.8 K [13].

In the hybrid cryocoolers, the recuperative coiled tube-in-tube heat exchanger (RCTTHE) is a key component, which not only acts as the carrier of heat transfer, but also plays an important role in energy recovery in the system [14]. On the other hand, the pressure drop at the low-pressure side is also critical to reduce the evaporative pressure for the JT cooler [9,13]. Thus, the optimizations of heat exchange and pressure drop at low-pressure side in the RCTTHE are crucial to decreasing the cooling temperature, increasing the cooling capacity and improving the cooling effectiveness of the hybrid cryocooler.

With the similar RCTTHE systems, Narasaki *et al.* [3] and Sato *et al.* [4] obtained a cooling power of 10 mW at 1.7 K based on the developed hybrid cryocooler with He-3 as the working medium in which the RCTTHE effectiveness was higher than 94 % and the pressure drop was 2.2 kPa. Petach *et al.* [6,7] and Crook *et al.* [8] achieved the no-load temperatures of 1.7 K and 2 K, respectively. However, previous researches mainly focused on the overall structures and the performances at the cold end. Little study was conducted on the characteristics of flow and heat transfer in the RCTTHE system.

* Corresponding author at: State Key Laboratory of Infrared Physics, Shanghai Institute of Technical Physics, Chinese Academy of Sciences, 500 Yutian Road, Shanghai 200083, China

E-mail address: haizheng.dang@mail.sitp.ac.cn (H. Dang).

https://doi.org/10.1016/j.cryogenics.2022.103535
Received 21 April 2022; Received in revised form 6 July 2022; Accepted 16 July 2022
Available online 21 July 2022
0011-2275/

Nomenclature

A_c	heat transfer area between low-pressure helium and separating wall (m^2)
$A_{c'}$	heat transfer area between low-pressure helium and external wall (m^2)
A_h	heat transfer area between high-pressure helium and separating wall (m^2)
A_o	radiant heat transfer area of external wall (m^2)
A_{sw}	heat conduction area of separating wall (m^2)
A_{ew}	heat conduction area of external wall (m^2)
C_p	isobaric specific heat (kJ kg^{-1} K^{-1})
D	Diameter of tube (m)
D_c	hydraulic diameter of low-pressure side (m)
D_h	hydraulic diameter of high-pressure side (m)
D_s	diameter of spiral coil (m)
f	friction coefficient (dimensionless)
Gz	Graetz number (dimensionless)
h	specific enthalpy (kJ kg^{-1})
L	length of tube (m)
IT	inertance tube
L^+	dimensionless length
ΔL	length of the i-th grid (m)
$\dot{m}$	mass flow rate (mg/s)
Nu	Nusselt number (dimensionless)
P	pressure (Pa)
per	Wetted perimeter (m)
Pr	Prandtl number (dimensionless)
PT	Pulse tube
Reg	regenerator
RCTTHE	recuperative coiled tube-in-tube heat exchanger
Re	Reynolds number (dimensionless)
T_C	cooling temperature (K)
T_H	ambient temperature (K)
T_{pre}	precooling temperature (K)
U_c	convective heat transfer coefficient between cold helium and wall (W m^{-2} K^{-1})
U_h	convective heat transfer coefficient between hot helium and wall (W m^{-2} K^{-1})
v	velocity (m/s)

Greeks

λ	thermal conductivity of wall (W/m K^{-1})
η	effectiveness of RCTTHE
ξ	local drag coefficient
κ	thermal conductivity of fluid (W/m K^{-1})
ρ	density (kg/m^3)
σ	Stefan-Boltzmann constant (W m^{-2} K^{-4})
τ	emissivity (dimensionless)
μ	dynamic viscosity of He-4 (Pa s)

Subscripts

1,2,3	thermodynamic states in Figs. 1 and 2
c	low-pressure cold helium
ew	external wall
h	high-pressure hot helium
s	spiral tube
sw	separating wall
w	wall

This paper develops a numerical model of the RCTTHE focusing on the flow and heat transfer characteristics for the 1.8 K hybrid cryocooler with He-4 as the only working medium. The governing equations of the high-pressure hot helium gas, the separating wall, the low-pressure cold helium gas and the external wall for flow and heat transfer in the RCTTHE were solved with a control volume finite difference method (CVFDM) [15]. In addition, the influence of radiant heat transfer is considered which has a great influence on low-temperature heat exchangers [16]. The empirical correlations for the flow and heat transfer of helium gas in different channels are also employed to solve the governing equations. The flow and heat transfer characteristics of the four-stage RCTTHE in a temperature range of 4–300 K are studied under different dimensional and operating parameters. In order to verify the theoretical analyses, the optimized four-stage RCTTHE system is designed and then integrated into the hybrid cryocooler. The experimental results are then compared with the theoretical analyses.

2. RCTTHE system

The 1.8 K hybrid cryocooler has been reported in our previous work [13]. Fig. 1 shows the overall schematic of the hybrid cryocooler, which is formed by a four-stage SPTC and a JTC and the two parts are thermally coupled with each other. The four-stage SPTC subsystem is driven by two moving-coil linear compressors, in which the first two stage are driven by one compressor while the last two stage by the other one. Besides the compressor, each stage of the SPTC consists of a regenerator, an inertance tube, a reservoir, a pulse tube and heat exchangers including warm and cold heads. The last three stage cold heads all serve as the precooling when coupled with the JTC to provide the precooling capacities of Q_{pre1}, Q_{pre2}, Q_{pre3} at three temperatures T_{pre1}, T_{pre2}, T_{pre3}, respectively [9,11,13].

The details of the JTC subsystem of the 1.8 K hybrid cryocooler are shown in Fig. 2. The subsystem mainly includes the four-stage JT compressors, the four-stage RCTTHE, the three-stage precooling heat exchangers (PHEXs), a JT valve, a bypass valve, and an evaporator. The four-stage RCTTHE are formed by four parts, namely, RCTTHE-1, RCTTHE-2, RCTTHE-3 and RCTTHE-4, which are put in between the four-stage JT compressors, the 1st stage PHEX, the 2nd stage PHEX, the 3rd stage PHEX and the JT valve in sequence, respectively. The heat transfer in the RCTTHE is realized by pumping the compressed helium gas up through a smaller tube put inside in a larger diameter return tube containing precooled helium. The precooling temperatures in the 1st, 2nd and 3rd stage PHEXs are 100, 40 and 10 K respectively. Fig. 3 shows that the *T-h* diagram of the JT subsystem with the three-stage precooling.

For the hybrid cryocooler with He-4 as the only working medium, in order to achieve a cooling temperature of below 2.0 K, the RCTTHE system has to meet the stringent requirements. For He-4, the saturation temperature of 2.0 K is corresponding to an evaporation pressure of 3.13 kPa, which indicates that the pressure after throttling should be lower than 3.13 kPa. Considering that the suction pressure provided by the actual JT compressor unit can only reach an ultimate low value 1.1 kPa [13], the pressure drops along the RCTTHE system, which must exist in reality, has to be lower than 2.03 kPa [13].

Based on the enthalpy flow model conducted in our previous work [11], the effect of the four-stage RCTTHE on the three-stage precooling capacities and the cooling capacity of the hybrid cryocooler can also be obtained, respectively.

Fig. 4 shows that the variations of the three-stage precooling capacities with the effectiveness of the RCTTHE. It is observed that the precooling capacities decrease monotonously with the increasing heat exchanger effectiveness.

Fig. 5 shows the effect of heat exchanger effectiveness of RCTTHE-4 on the cooling capacity of the hybrid cryocooler at 1.8 K. It is observed

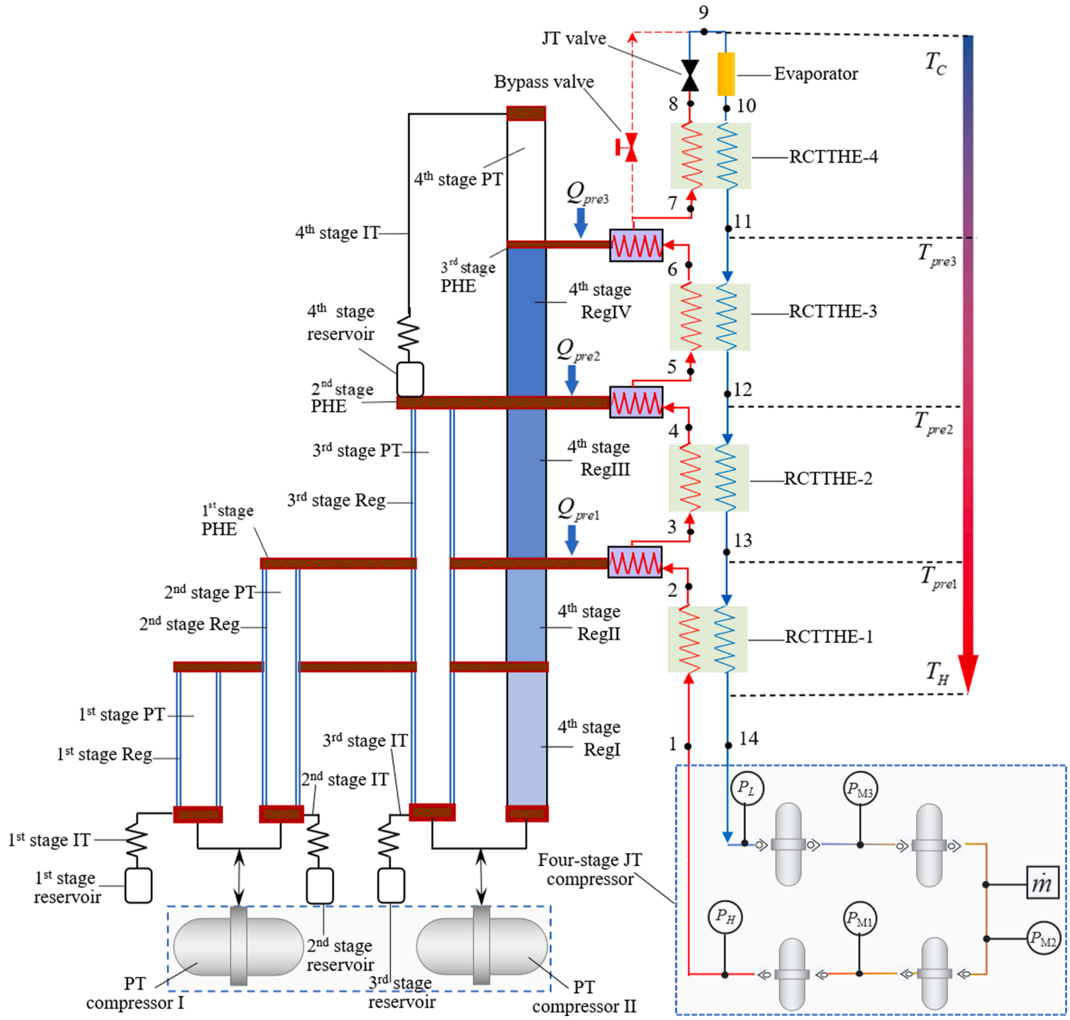

Fig. 1. Schematic of the 1.8 K hybrid cryocooler.

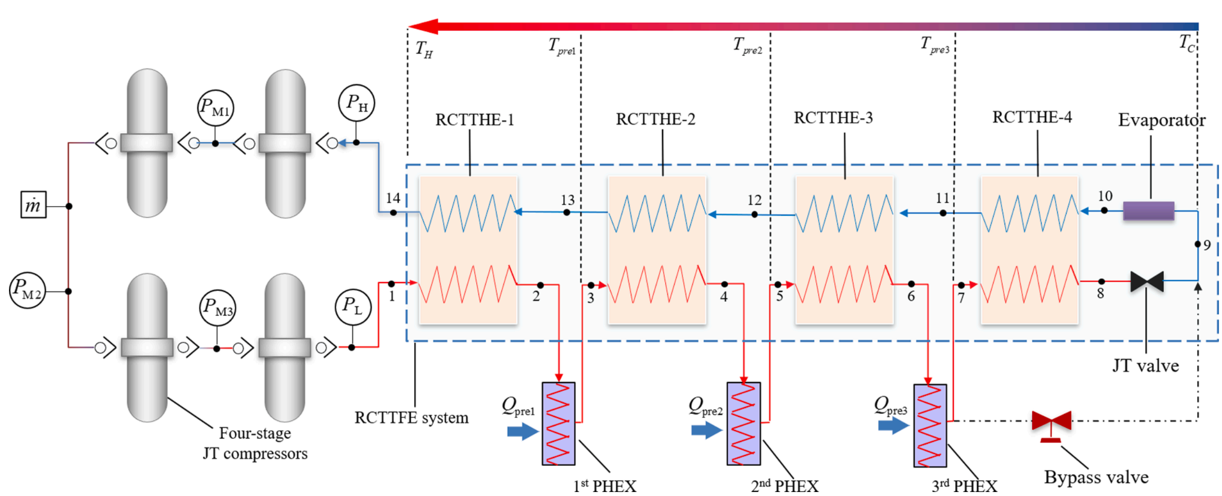

Fig. 2. Schematic of the JT cooler structure and cycle flow of the RCTTHE system.

that the cooling capacity increases linearly with the effectiveness of RCTTHE-4 for each the third-stage precooling temperature (T_{pre3}). On the other hand, the zero-points of the cooling capacity are 87.8 %, 92.7 %, and 95.2 % for the given third-stage precooling temperature of 10 K, 12 K, 14 K, respectively, which indicates that for a higher T_{pre3}, the effectiveness of RCTTHE-4 has to be enhanced considerably in order to obtain the necessary cooling capacity for the hybrid cryocooler.

3. RCTTHE design

Compared with the conventional RCTTHE with a fixed inlet temperature, the RCTTHE in the hybrid cryocooler also has the feature that

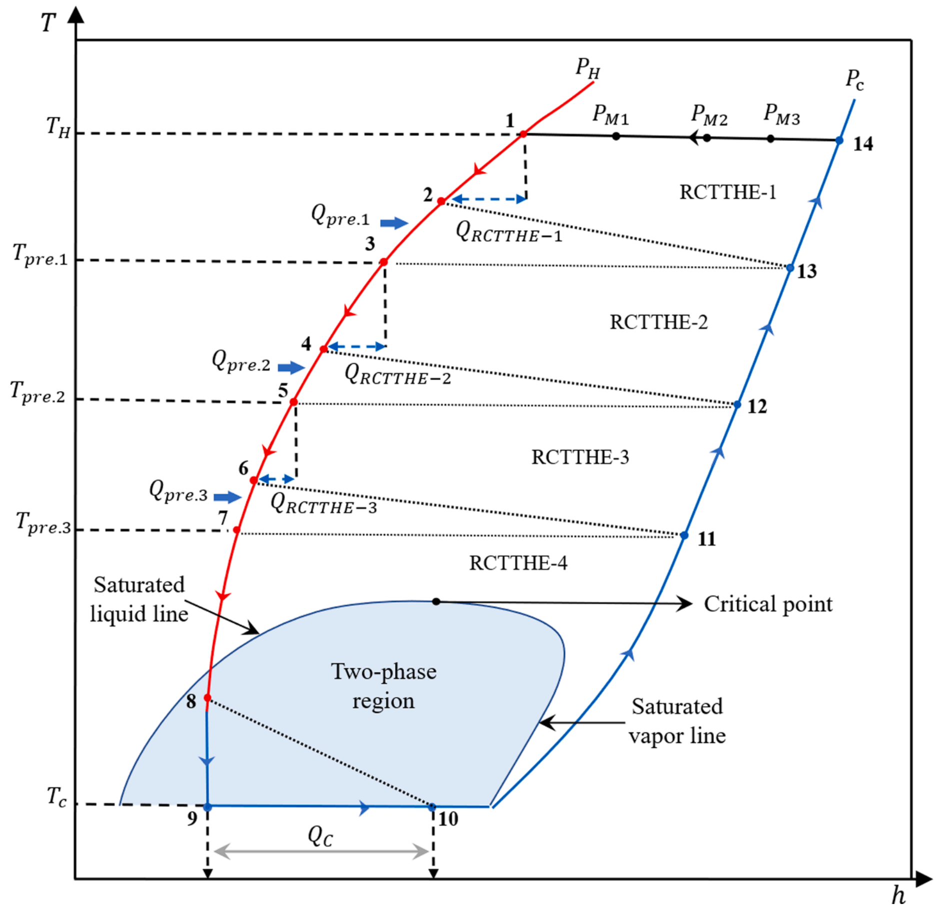

Fig. 3. JT cycle of hybrid cryocooler in *T*-h thermodynamic plane.

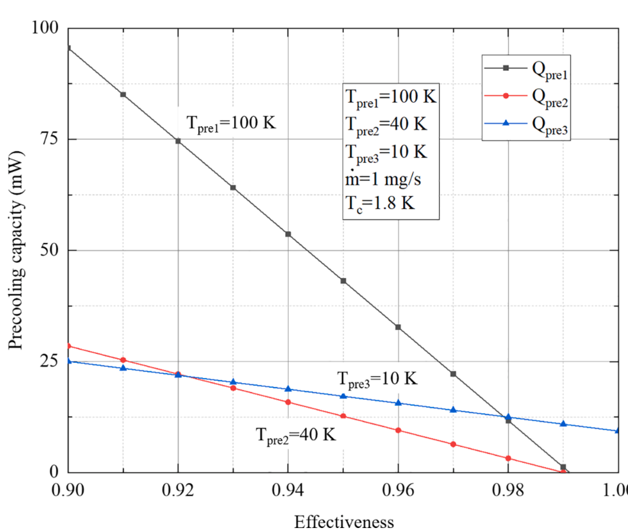

Fig. 4. Effect of heat transfer effectiveness on precooling capacity.

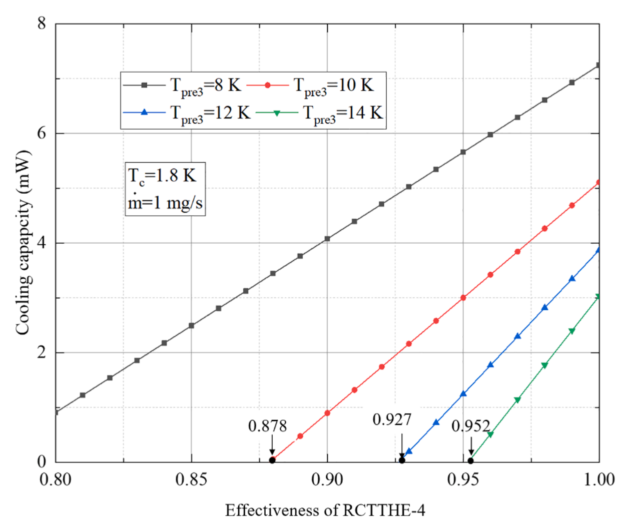

Fig. 5. Effect of heat transfer effectiveness for RCTTHE-4 on cooling capacity in the 1.8 K hybrid cryocooler at various T_{pre3}.

during operation, the inlet temperature at either cold or hot end will continue to decrease until it reaches the final equilibrium state. For He-4, its thermal properties change significantly with the temperature in 4 to 300 K. The variations of density, specific heat, dynamic viscosity and thermal conductivity with temperature under two given pressures of 1.618 kPa and 0.3 MPa are shown in Fig. 6. For the reported 1.8 K hybrid cryocooler, the typical temperature regions of the four-stage RCTTHE are 100–300 K, 40–100 K, 10–40 K and 4.2–10 K, respectively.

In our design, the thin-walled stainless steel is used as the material of the RCTTHE to minimize the heat leakage between the hot and cold end, and also to provide appropriate heat transfer between the high-pressure and low-pressure helium of the RCTTHE [17]. Fig. 7 shows the inner details of the RCTTHE.

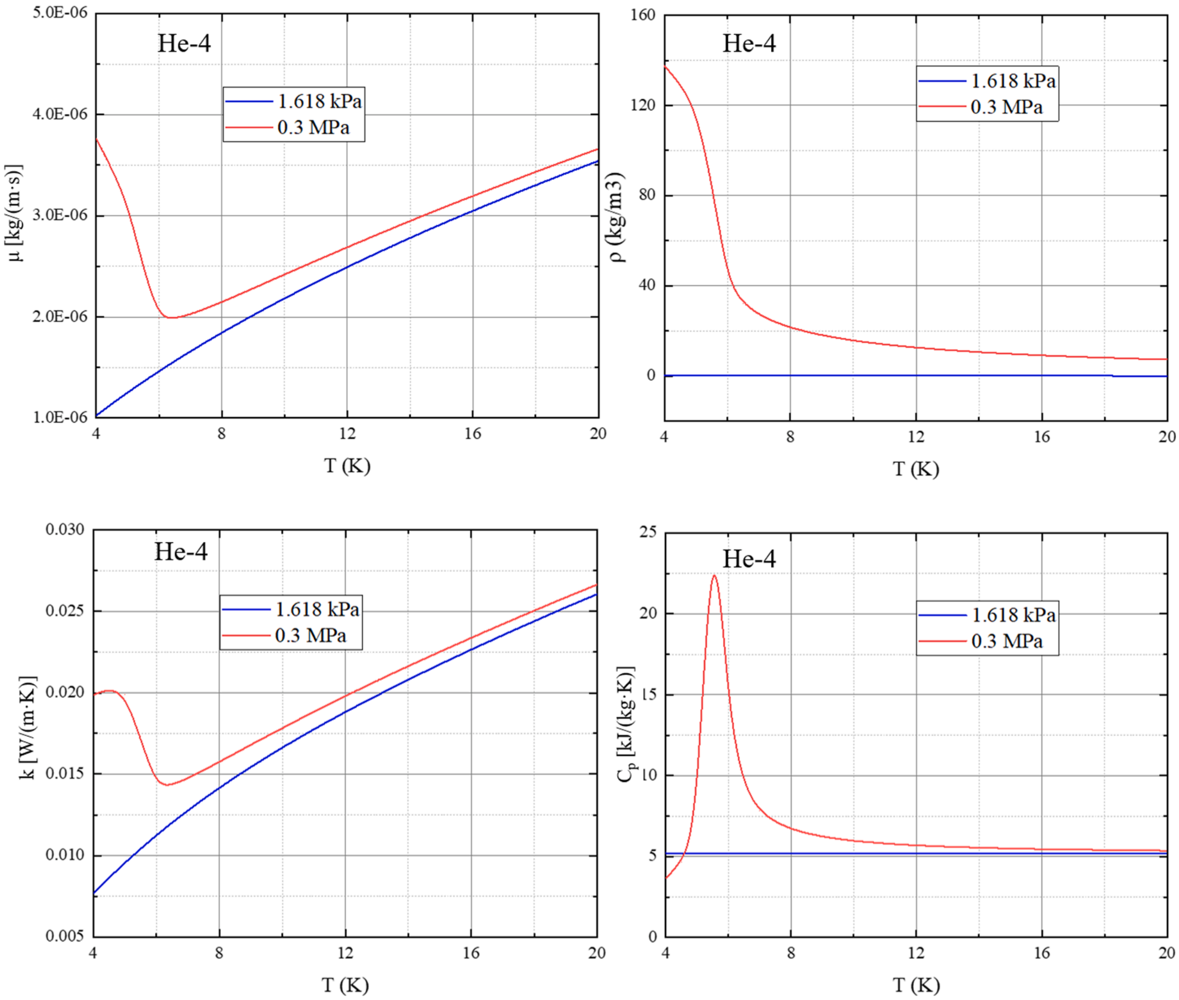

Fig. 6. Physical properties of He-4 versus temperature of 4–20 K at 1.618 kPa and 0.3 MPa.

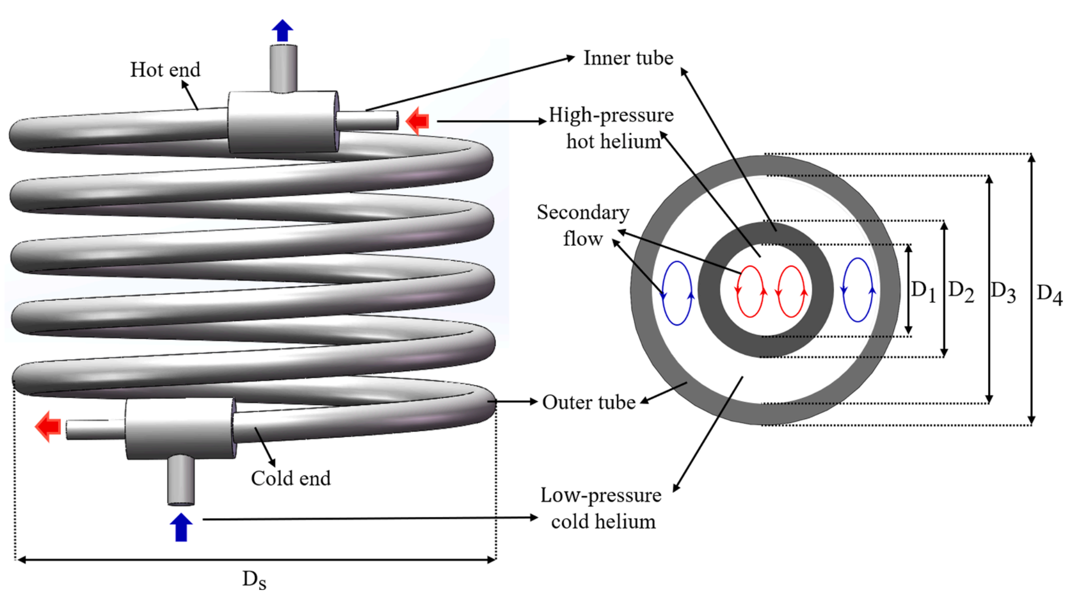

Fig. 7. Schematic of the RCTTHE and stream configuration.

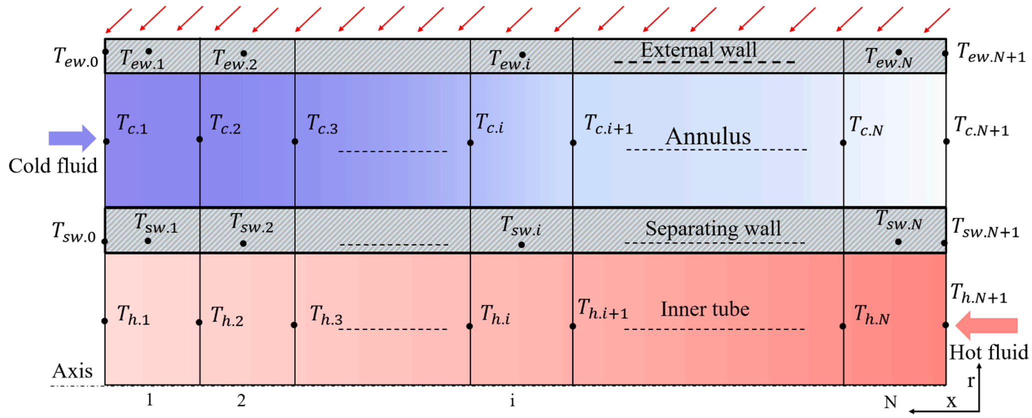

Fig. 8. Computational grid of the RCTTHE.

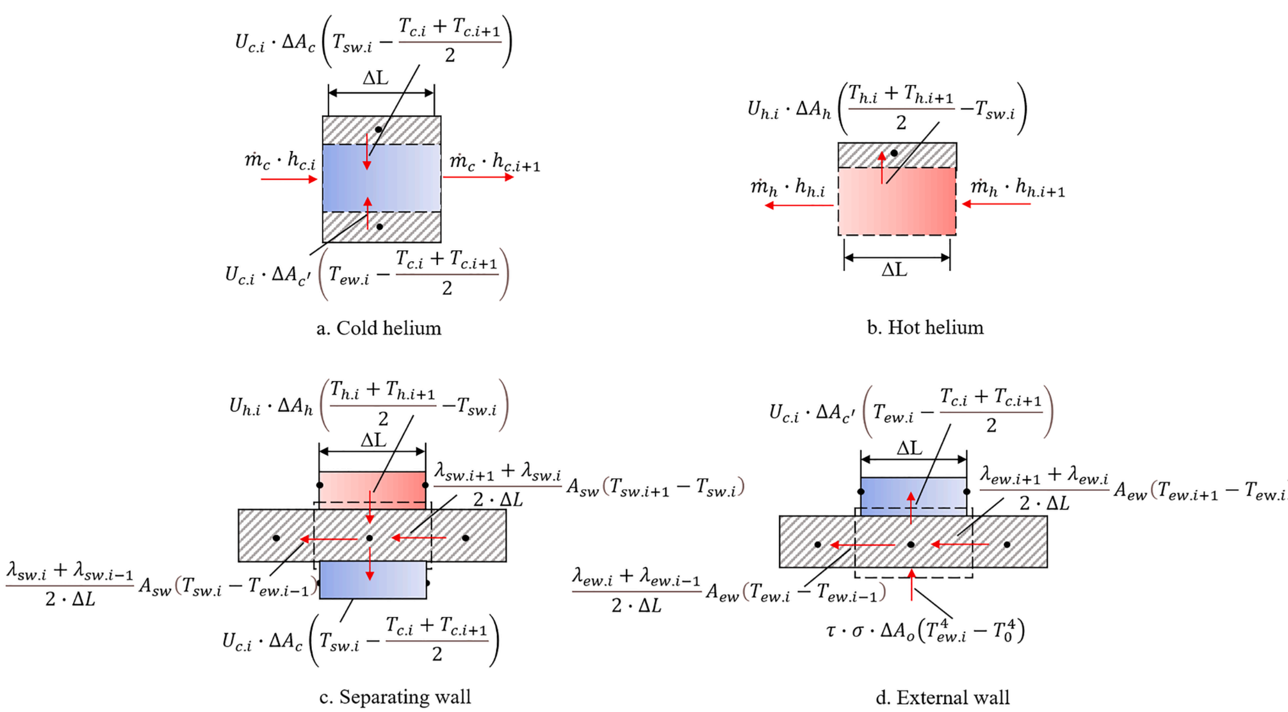

Fig. 9. Control volume and energy flows for the i-th section of the RCTTHE.

3.1. Heat transfer model

3.1.1. Assumptions

The following assumptions are made in the model:

(1) The flow in the RCTTHE is one-dimensional steady-state.
(2) The conduction resistance in radial direction of heat exchanger is negligible compared to that of convection resistance.
(3) In the flow direction, the energy exchange produced by the heat conduction of the fluid is negligible compared with that by the heat convection.

3.1.2. Governing equations

Fig. 8 shows that the RCTTHE is divided into N identical grids. For the i-th grid, the energy conservation equations under steady state condition are established for low-pressure cold helium, high-pressure hot helium, separating wall, and external wall. Fig. 9 illustrates the control volume and energy flows for the low-pressure cold helium, the high-pressure hot helium, the separating wall and the external wall in the i-th section of the RCTTHE, respectively.

For low-pressure cold helium:

$$\dot{m}_c \bullet h_{c.i} + U_{c.i} \bullet \Delta A_{c'} \left(T_{ew.i} - \frac{T_{c.i} + T_{c.i+1}}{2} \right) = \dot{m}_c \bullet h_{c.i+1} - U_{c.i} \bullet \Delta A_c \left(T_{sw.i} - \frac{T_{c.i} + T_{c.i+1}}{2} \right) \tag{1}$$

For high-pressure hot helium:

$$\dot{m}_h \Delta h_{h.i} = \dot{m}_h \Delta h_{h.i+1} - U_{h.i} \cdot \Delta A_h \left(\frac{T_{h.i} + T_{h.i+1}}{2} - T_{sw.i} \right) \tag{2}$$

For separating wall:

$$\frac{\lambda_{sw.i+1} + \lambda_{sw.i}}{2\Delta L} A_{sw} (T_{sw.i+1} - T_{sw.i}) + U_{h.i} \cdot \Delta A_h \left(\frac{T_{h.i} + T_{h.i+1}}{2} - T_{sw.i} \right) = \frac{\lambda_{sw.i} + \lambda_{sw.i-1}}{2\Delta L} A_{sw} (T_{sw.i} - T_{sw.i-1}) + U_{c.i} \cdot \Delta A_c \left(T_{sw.i} - \frac{T_{c.i} + T_{c.i+1}}{2} \right) \tag{3}$$

For external wall:

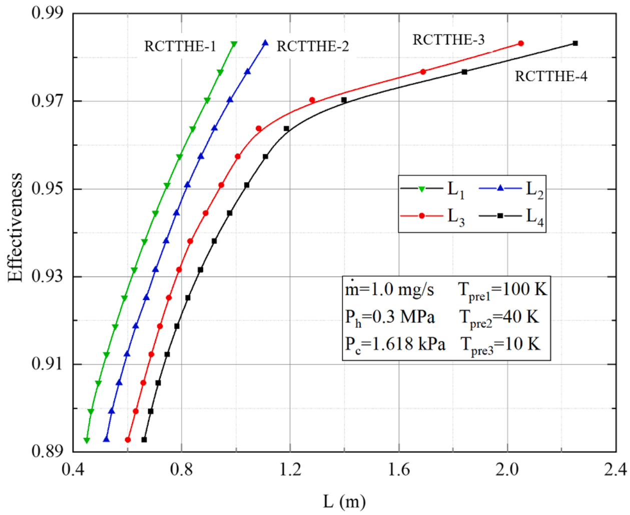

Fig. 10. Change of length for four-stage RCTTHEs with heat exchanger effectiveness.

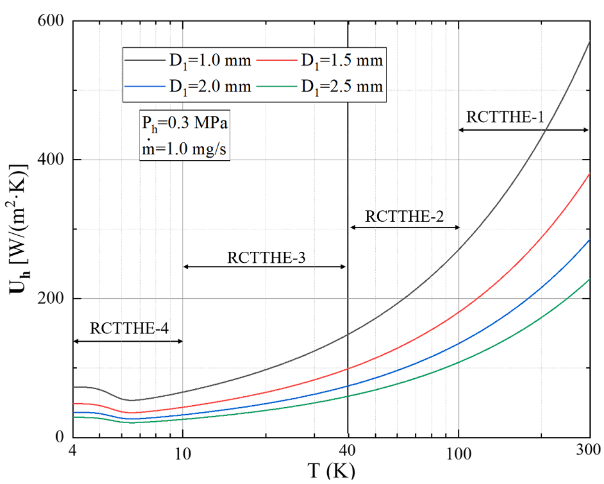

Fig. 11. Effect of heat transfer coefficient at the high-pressure side on temperature with different inner diameter of inner tube.

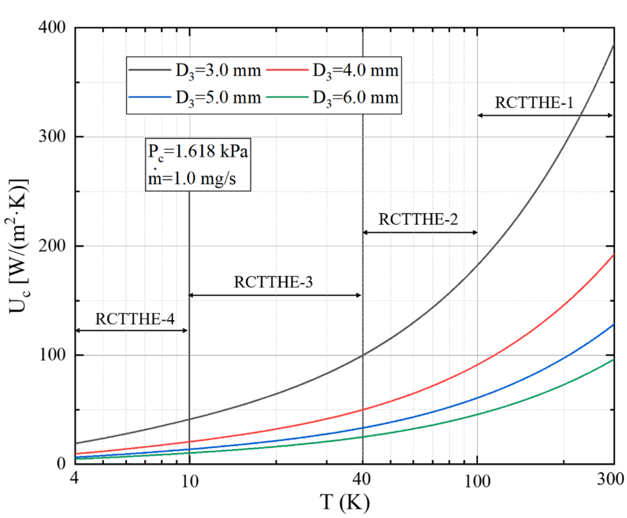

Fig. 12. Effect of heat transfer coefficient at the low-pressure side on temperature with different inner diameter of outer tube.

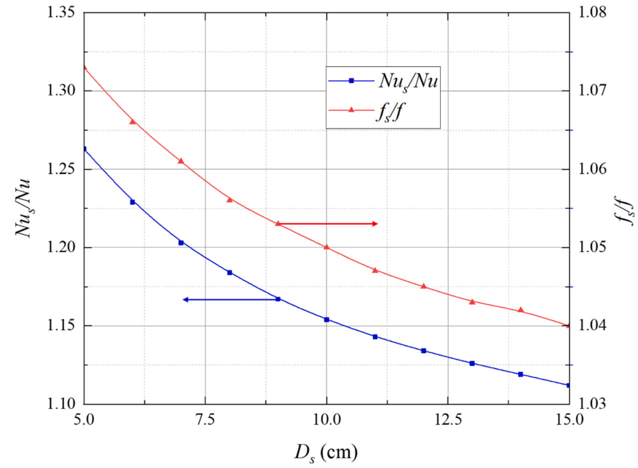

Fig. 13. Changes of Nu_s/Nu and f_s/f with different D_s.

$$\frac{\lambda_{ew.i+1}+\lambda_{ew.i}}{2\Delta L}A_{ew}(T_{ew.i+1}-T_{ew.i})+\tau\Delta\sigma\cdot\Delta A_o\left(T_{ew.i}^4-T_0^4\right)$$
$$=\frac{\lambda_{ew.i}+\lambda_{ew.i-1}}{2\Delta L}A_{ew}(T_{ew.i}-T_{ew.i-1})+U_{c.i}\cdot\Delta A_c^{\prime}\left(T_{ew.i}-\frac{T_{c.i}+T_{c.i+1}}{2}\right) \quad (4)$$

where $\dot{m}_c$ is the mass flow rate of low-pressure cold helium, $\dot{m}_h$ is the mass flow rate of high-pressure hot helium, $h_{c.i}$ is the low-pressure cold helium specific enthalpy of the i-th grid. $h_{h.i}$ is the high-pressure hot helium specific enthalpy of the i-th grid. $U_{c.i}$ is the convective heat transfer coefficient of the i-th grid between wall and low-pressure cold helium. $U_{h.i}$ is the convective heat transfer coefficient of the i-th grid between wall and high-pressure hot helium. ΔA_c is the heat transfer area between separating wall and low-pressure cold helium. ΔA_c' is the heat transfer area between external wall and low-pressure cold helium. ΔA_h is the heat transfer area between separating wall and high-pressure hot helium. A_{ew} is the heat conduction area of external wall. A_{sw} is the heat conduction area of the separating wall. ΔA_o is the radiant heat transfer area of external wall. $\lambda_{sw.i}$ is the stainless steel thermal conductivity of the i-th grid about separating wall. $\lambda_{ew.i}$ is the stainless steel thermal conductivity of the i-th grid about external wall. ΔL is the length of the i-th grid. τ is the emissivity of external wall. σ is the Stefan-Boltzmann constant.

3.1.3. Boundary conditions

For the energy equations, the inlet temperatures for high-pressure helium and low-pressure helium are given in Eqs. (5) and (6), respectively. The adiabatic boundary conditions are used to the cold and the hot ends of wall as given in Eqs. (7)–(10).

$$T_c = T_{c.1} \quad (5)$$

$$T_h = T_{h.N+1} \quad (6)$$

$$T_{sw.0} = T_{sw.1} \quad (7)$$

$$T_{sw.N} = T_{sw.N+1} \quad (8)$$

$$T_{ew.0} = T_{ew.1} \quad (9)$$

$$T_{ew.N} = T_{ew.N+1} \quad (10)$$

Eqs. (1)–(10) are solved over the control volume.

3.1.4. Calculations of geometry

The heat transfer areas between low-pressure helium and external wall, between low-pressure helium and separating wall, and between high-pressure helium and separating wall are given in Eqs. (11)–(13), respectively, as shown in Fig. 7:

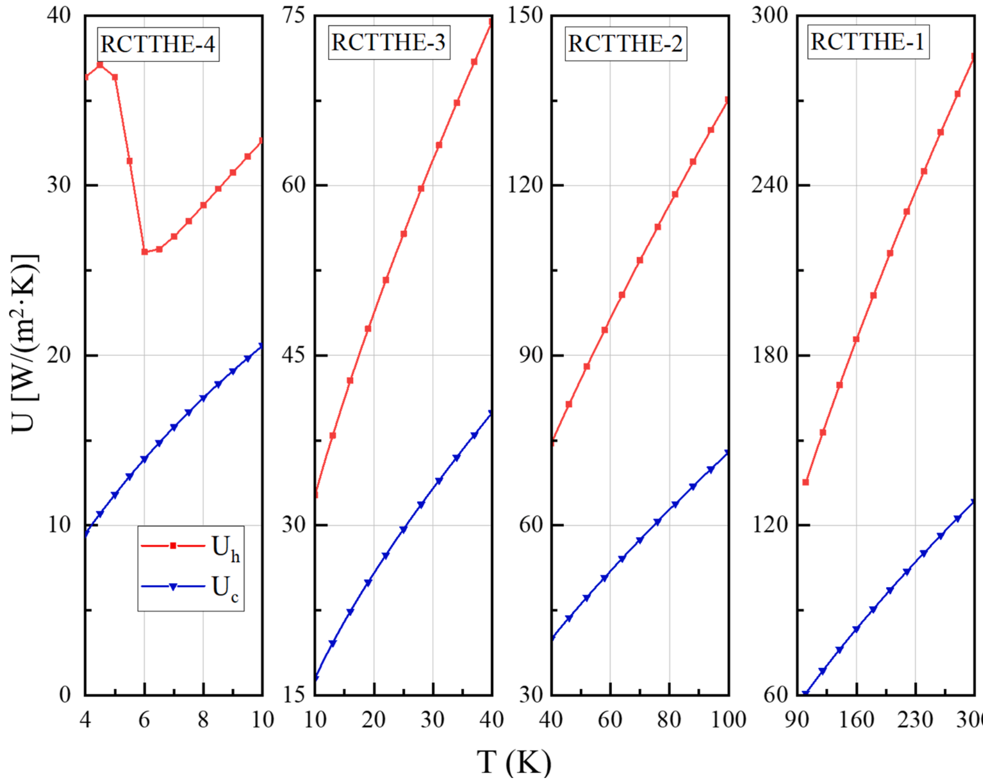

Fig. 14. Change of heat transfer coefficient at low-pressure and high-pressure side with temperature in the four-stage RCTTHE.

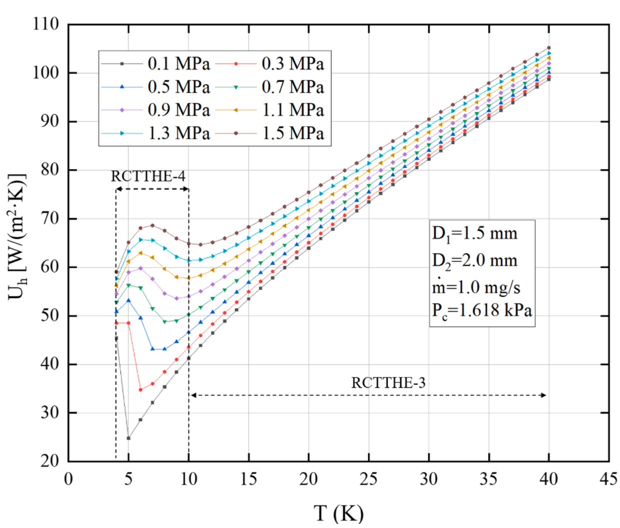

Fig. 15. Change of heat transfer coefficient at high-pressure side with temperature of 4–40 K in different high-pressure.

$$\Delta A_{c'} = \pi D_3 \Delta L \tag{11}$$

$$\Delta A_c = \pi D_2 \Delta L \tag{12}$$

$$\Delta A_h = \pi D_1 \Delta L \tag{13}$$

The radiant heat transfer area of external wall is given as follow:

$$\Delta A_o = \pi D_4 \Delta L \tag{14}$$

The heat conduction area of separating wall is given as follow:

$$A_{sw} = \frac{\pi}{4}(D_2^2 - D_1^2) \tag{15}$$

The heat conduction area of external wall is given as follow:

$$A_{ew} = \frac{\pi}{4}(D_4^2 - D_3^2) \tag{16}$$

The length of the i-th grid is defined as:

$$\Delta L = \frac{L}{N} \tag{17}$$

where D_1 is the inner diameter of inner tube. D_2 is the outer diameter of inner tube. D_3 is the inner diameter of outer tube. D_4 is the outer diameter of outer tube. L is the length of the RCTTHE. N is the number of grids.

3.1.5. Heat transfer correlations

The convective heat transfer coefficient between high-pressure hot helium and separating wall is:

$$U_h = \frac{Nu_h \kappa_h}{D_h} \tag{18}$$

where κ_h is the thermal conductivity of high-pressure hot helium. D_h is the hydraulic diameter of high-pressure channel ($D_h = 4A_h/per_h$). per_h is the wetted perimeter of high-pressure channel. Nu_h is Nusselt number for high-pressure side, which is given as [18,19]:

$$Nu_h = 3.66 + \frac{\left(0.049 + \frac{0.020}{Pr_h}\right)Gz^{1.12}}{\left(1 + 0.065Gz^{0.7}\right)} \tag{19}$$

$$Gz = \frac{D_h Re_h Pr_h}{L} \tag{20}$$

where Gz is the Graetz number. Re_h is the Reynolds number of high-pressure side based on the hydraulic diameter. $Pr_h = \mu_h C_{p.h}/\kappa_h$ is the Prandtl number of high-pressure hot helium. $C_{p.h}$ is the isobaric specific heat of high-pressure hot helium. μ_h is the dynamic viscosity of high-pressure hot helium. A_h is the cross-sectional area of high-pressure

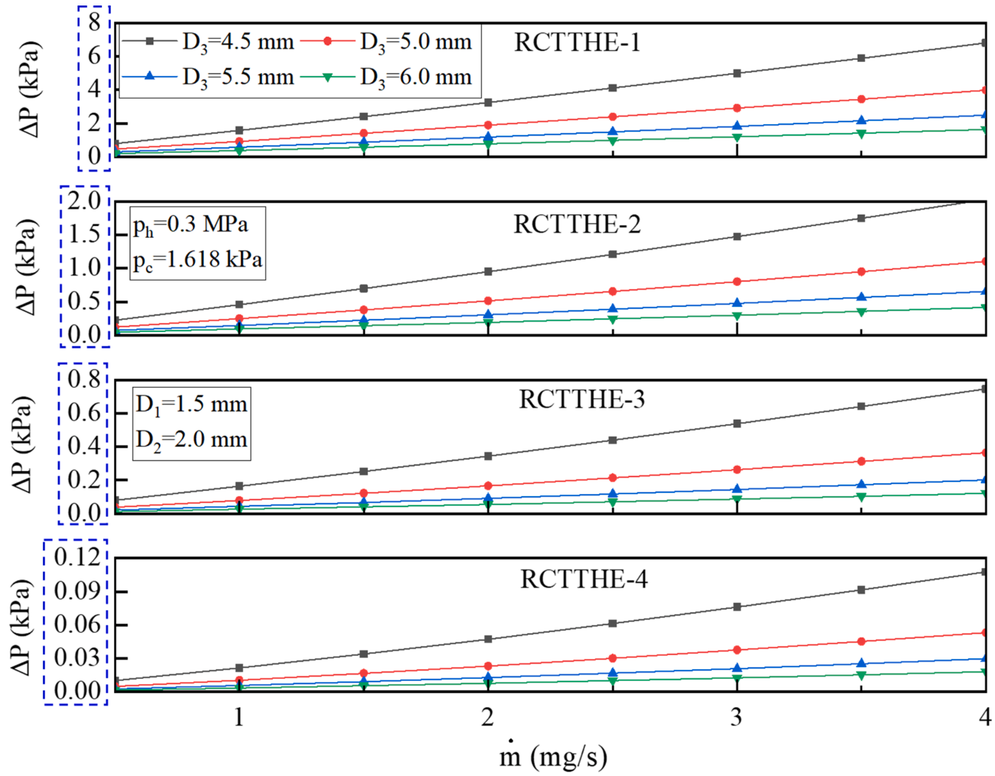

Fig. 16. Change of pressure drop for four-stage RCTTHE with mass flow rate in different inner diameter of outer tube.

Table 1
Structural parameters of four-stage RCTTHE.

Heat exchanger	Structural parameters				RCTTHE effectiveness (simulation)	RCTTHE effectiveness (experimental)
	Inner tube	Outer tube	D_s (mm)	Length (m)		
RCTTHE −1	$D_1 = 1.5$ mm $D_2 = 2.0$ mm	$D_3 = 6.0$ mm $D_4 = 6.5$ mm	80	$L_1 = 0.96$	97.2 %	98.1 %
RCTTHE −2	$D_1 = 1.5$ mm $D_2 = 2.0$ mm	$D_3 = 5.5$ mm $D_4 = 6.0$ mm	80	$L_2 = 1.0$	97.1 %	97.8 %
RCTTHE −3	$D_1 = 1.5$ mm $D_2 = 2.0$ mm	$D_3 = 5.0$ mm $D_4 = 5.5$ mm	50	$L_3 = 1.28$	97.0 %	97.3 %
RCTTHE −4	$D_1 = 1.5$ mm $D_2 = 2.0$ mm	$D_3 = 4.5$ mm $D_4 = 5.0$ mm	50	$L_4 = 1.3$	96.9 %	97.1 %

channel.

Eqs. (18)–(20) are solved to the convection heat transfer coefficient between high-pressure hot helium and separating wall.

The convection heat transfer coefficient between low-pressure cold helium and wall is:

$$U_c = \frac{Nu_c \kappa_c}{D_c} \tag{21}$$

where κ_c is the thermal conductivity of low-pressure cold helium. D_c is the hydraulic diameter of low-pressure channel, $D_c = 4A_c/per_c$. A_c is the cross-sectional area of low-pressure channel. per_c is the wetted perimeter of low-pressure channel. Nu_c is the Nusselt number for low-pressure cold helium, which is given as [18,19]:

$$Nu_c = Nu_{fd} + DNurat \times DNu \tag{22}$$

where Nu_{fd} is the Nusselt number with the boundary layer in the fully developed situation of flowing, $DNurat$ is the correction factor, DNu is the influence of the entrance section when $Pr_c = 0.72$.

$$Nu_{fd} = \frac{0.580342564}{RR} + 6.09483719 - 4.45569753 \times RR + 2.64812415 \times RR^2 \tag{23}$$

$$DNurat = \begin{cases} 0.6847 + 0.3153 \times e^{-1.26544559 \times (ln(Pr_c) - ln(0.72)}\ Pr_c > 0.72 \\ 1.68 + 0.68 \times e^{0.32 \times (ln(Pr_c) - ln(0.72)}\ Pr_c \le 0.72 \end{cases} \tag{24}$$

$$DNu = 1.75450933 \times e^{[-0.402783707 \times \ln(\frac{L}{D_c Re_c Pr})]^{1.050}} \tag{25}$$

where $Pr_c = \mu_c C_{p.c}/\kappa_c$ is the Prandtl number of low-pressure cold helium. $C_{p.c}$ is the isobaric specific heat of low-pressure cold helium. μ_c is the dynamic viscosity of low-pressure helium. RR is the ratio of the inner to the outer radius of the annulus channel [18,19].

Eqs. (21)–(25) are solved to the convection heat transfer coefficient between wall and low-pressure cold helium.

Eqs. (18)–(25) are used to calculate the heat transfer coefficient in a straight tube. However, the flow of helium in a spiral tube is more complicated than that in a straight tube. The changing direction of the fluid increases the disturbance of helium in the tube, thereby enhancing the heat transfer and friction resistance between helium and wall. For

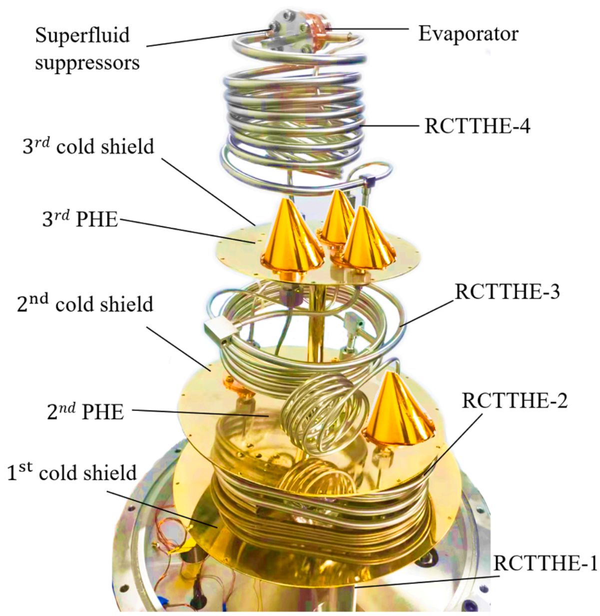

Fig. 17. Physical map of optimized RCTTHE system.

different spiral diameters D_s, the following formula can be used to correct the heat transfer problem in the spiral tube [17].

$$\frac{Nu_s}{Nu} = 1 + 3.6(1 - \frac{D}{D_s})(\frac{D}{D_s})^{0.8} \tag{26}$$

where D is the inner diameter of high-pressure tube. Nu_s is the Nusselt number of the spiral tube. D_s is the spiral diameters.

3.2. Flow model

In general, the pressure drops of the RCTTHE are divided into the pressure drop along the channel and the local pressure drop, in which the former is mainly caused by the frictional resistance while the latter by the flow passing through the variable diameter channel or changing the flow direction. The local pressure drop of RCTTHE occurs at the three-way at the inlet and outlet of the heat exchanger.

Eqs. (28)–(33) are given as follows to calculate the pressure drop of

Table 2
Details of the measuring sensors.

Sensor	Measuring range	Uncertainty	Brand/type
Thermometer	1.4 ~ 325 K	±4 mK	Cernox 1050
Pressure sensor	0–5 MPa	±1.4 %	Kistler 4043A
Mass flow rate meter	0 ~ 8.4 mg/s	0.1 mg/s	OMEGA

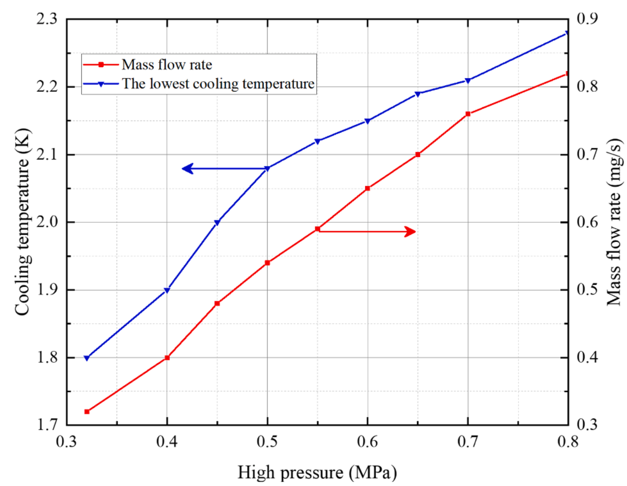

Fig. 19. Experimental results of effect of high-pressure on mass flow rate and cooling temperature.

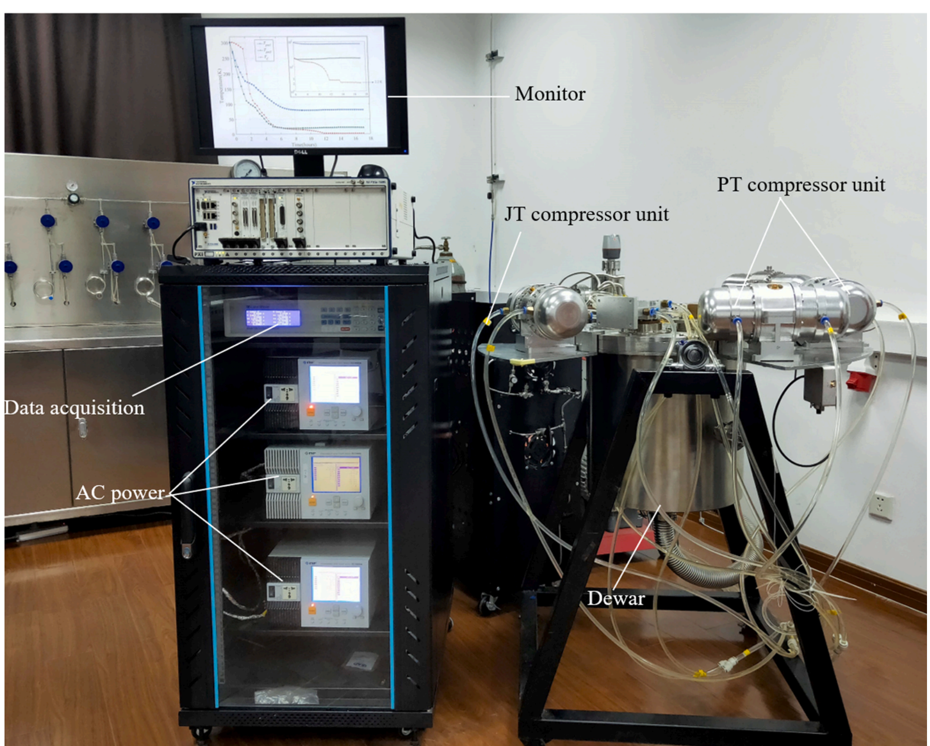

Fig. 18. Experimental set up of 1.8 K hybrid cryocooler based on the optimized RCTTHE system.

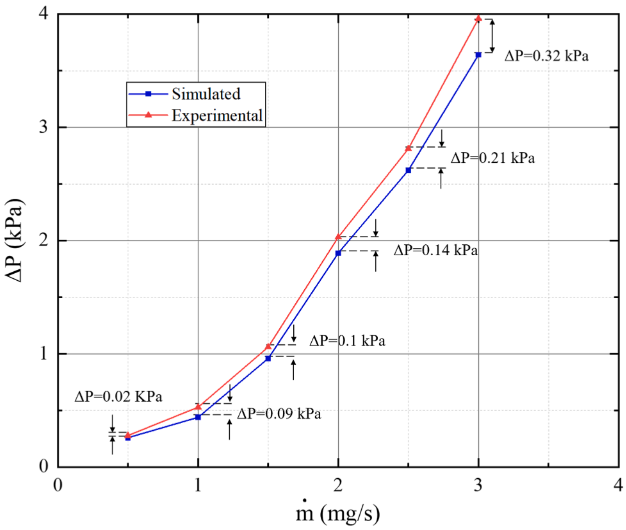

Fig. 20. Results of ΔP_c by calculated and measured in different mass flow rate.

RCTTHE.

$$\Delta P = \Delta P_a + \Delta P_l \tag{27}$$

where ΔP_a is the pressure drop along the channel of RCTTHE and ΔP_l is the local pressure drop, which are given as follows:

$$\Delta P_a = f \cdot \frac{L}{D} \cdot \frac{\rho v^2}{2} \tag{28}$$

$$\Delta P_l = \xi \cdot \frac{\rho v^2}{2} \tag{29}$$

where ξ is the local resistance coefficient [20]. f is the coefficient of friction which depends on the channel fluid flows and fluid properties, and its value at the high-pressure side is given by [18,19]:

$$f_{fd.h} = \frac{4}{Re_h}\left[\frac{3.44}{\sqrt{L^+}} + \frac{\frac{1.25}{4L^+} + 16 - \frac{3.44}{\sqrt{L^+}}}{1 + \frac{0.00021}{(L^+)^2}}\right] \tag{30}$$

where $f_{fd.h}$ is the friction coefficient of high-pressure side in straight tube. L^+ is the dimensionless length.

$$L^+ = \frac{L}{D_h Re_h} \tag{31}$$

The friction coefficient of the low-pressure side is given as:

$$f_{fd.l} = \frac{64}{Re_c}\sqrt{\frac{(1 - RR^2)}{1 + RR^2 - \left(\frac{1 - RR^2}{ln(RR^{-1})}\right)}} \tag{32}$$

where $f_{fd.l}$ is the friction coefficient of low-pressure side in straight tube.

Eqs. (28)–(33) are used to calculate the pressure drop in straight tube. Correspondingly, the friction coefficient in the spiral tube should also be corrected. For different spiral diameters, the following formula can be used to correct the flow problem in the spiral tube [17].

$$\frac{f_s}{f_{fd}} = 1 + 0.0823\left(1 + \frac{D}{D_s}\right)\left(\frac{D}{D_s}\right)^{0.53} Re^{0.25} \tag{33}$$

where f_s is the friction coefficient of the spiral tube.

3.3. Heat exchanger effectiveness

According to the definition of effectiveness, the effectiveness of a heat exchanger is the ratio of the actual heat transfer to the maximum possible value. Since the isobaric specific heat of helium varies greatly with temperature, as shown in Fig. 6, the conventional calculation methods based on the temperature difference can not be used to calculate the RCTTHE effectiveness. Therefore, the enthalpy difference

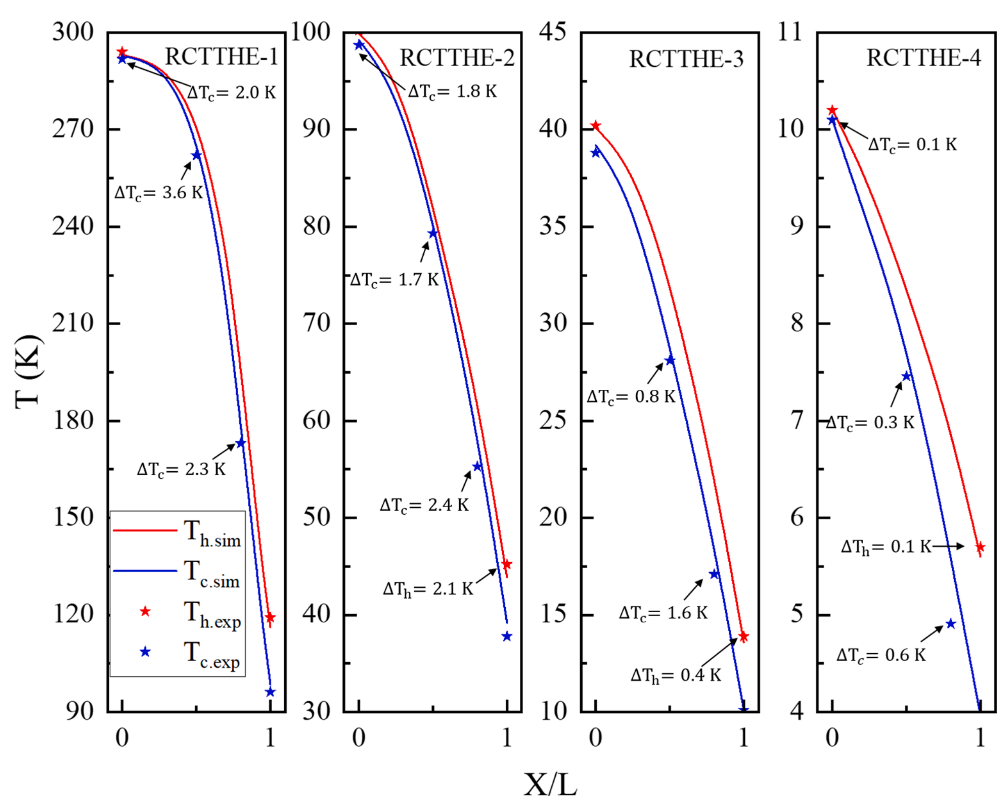

Fig. 21. Results of temperature profiles by calculated and measured along the tube of the four-stage RCTTHE (total length is L).

should be used to express the effectiveness. The heat exchanger effectiveness can be defined based on the minimum heat capacity of helium. If the high-pressure helium is the minimum heat capacity rate fluid, the heat exchanger effectiveness is defined by [17]:

$$\varepsilon_h = \frac{\dot{Q}_h}{\dot{Q}_{h.max}} = \frac{\dot{m}[h(T_{h,N+1}, P_h) - h(T_{h,1}, P_h)]}{\dot{m}[h(T_{h,N+1}, P_h) - h(T_{c,1}, P_h)]} \tag{34}$$

Similarly, If the low-pressure helium is the minimum heat capacity rate fluid, the heat exchanger effectiveness is defined by [17]:

$$\varepsilon_c = \frac{\dot{Q}_c}{\dot{Q}_{c.max}} = \frac{\dot{m}\left[h\left(T_{c,N+1}, P_c\right) - h\left(T_{c,1}, P_c\right)\right]}{\dot{m}\left[h\left(T_{c,N+1}, P_c\right) - h\left(T_{h,1}, P_c\right)\right]} \tag{35}$$

where P_h is the high pressure. P_c is the low pressure.

4. Optimization of RCTTHE

4.1. Heat transfer

4.1.1. Effect of geometry on heat exchanger coefficient

The heat transfer area and the heat transfer coefficient are two key factors that affect heat exchanger effectiveness. The heat transfer area is determined by the structural parameters such as the length and diameter of the heat exchange tube, while the heat transfer coefficient is related to the fluid velocity and its thermophysical properties.

Fig. 10 shows that the effect of the length of heat exchanger on its effectiveness. L_1, L_2, L_3 and L_4 represent the length of RCTTHE-1, RCTTHE-2, RCTTHE-3 and RCTTHE-4, respectively. It is observed that the effectiveness of the four-stage RCTTHE will increase as the increasing length. When the heat exchange area reaches a certain value with the corresponding effectiveness of 97 %, for the RCTTHE-3 and the RCTTHE-4, it is not appropriate to improve the heat exchange effectiveness by increasing the heat exchange area. In other words, to increase the length of heat exchange is no longer obvious in improving the heat exchanger effectiveness. Therefore, the heat transfer coefficient should be considered as a major measure to enhance the heat exchanger effectiveness.

From the above Eqs. (18)–(20), U_h is determined by:

$$U_h = 3.36\frac{k_h}{D_h} + \frac{0.049(\rho_h v_h C_p)^{1.12}\mu_h + 0.02k_h(\rho_h v_h D_h)^{1.12}C_p^{\,0.12}}{k_h^{1.12}\mu_h + 0.065\mu_h k_h^{0.42}(\rho_h v_h C_p D_h)^{0.7}} \tag{36}$$

where the first item on the right is much larger than the second one [19]. Thus, the heat transfer coefficient at the high-pressure side can be approximated as inversely proportional to diameter while proportional to thermal conductivity.

Fig. 11 shows the effect of temperature on the heat transfer coefficient of the RCTTHE with the different inner diameter of the inner tube. The coefficient increases with the decreasing inner diameter. It is also observed that the heat transfer coefficient on the high-pressure side increases with the increasing temperature in RCTTHE-1, RCTTHE-2 and RCTTHE-3. However, in RCTTHE-4, the heat transfer coefficient first decreases and then increases with the increasing temperature, and there is a minimum value of coefficient which is around 6.5 K. The reason is that there is a concave change of the thermal conductivity for He-4 with a pressure of 0.3 MPa at around 6.5 K, as shown in Fig. 6. The drastic decrease of the thermal conductivity causes a reduction of heat transfer coefficient at the high-pressure side.

Fig. 12 shows that the heat transfer coefficient on the low-pressure side versus temperature with different inner diameters of the outer tube. The coefficient increases with the decreasing of inner diameter. This is due to the fact that the velocity of helium increases as the cross-sectional area decreases, thereby enhancing the heat transfer coefficient. On the other hand, the heat transfer coefficient decreases with the decreasing temperature for the same structure channel.

In summary, based on Figs. 11 and 12, it is observed that the heat transfer coefficient changes considerably with the variations of the temperature. Therefore, the changing temperature must be considered as an important factor when the heat exchange area is calculated, since a large error would occur if the heat exchange area is still calculated by a constant heat transfer coefficient according to the conventional method [7,15,18]. On the other hand, reducing the diameter of the heat exchange tube can enhance the heat transfer coefficient.

The studied four-stage RCTTHE are coiled and wound around the cylinder of the cold head of the precooler, which can not only make the RCTTHE system compact, but also improve the heat transfer performance of the heat exchanger. As shown in Fig. 7, the curvature (D/D_S) in the RCTTHE creates a secondary flow, whose direction is perpendicular to the direction of primary helium flow. D is the diameter of the heat exchange tube, and herein it is equal to D_3. This secondary flow improves the heat transfer coefficient and also increases the friction coefficient between the wall and the flowing helium [17,19]. Fig. 13, based on Eqs. (26) and (33), aims at investigating the effect of D_s on the RCTTHE performance. It is observed that both Nu and f increase with the decrease of D_s. Nu_s/Nu increases from 1.12 to 1.26 and f_s/f rises from 1.04 to 1.07 when the spiral diameters D_s is reduced from 15 cm to 5 cm, which means that reducing the spiral diameters can enhance both heat transfer coefficient and friction coefficient. Therefore, within the required pressure drop range, D_s should be reduced as much as possible to enhance heat transfer and make the RCTTHE system more compact.

4.1.2. Effect of operating parameters on heat exchanger coefficient

Fig. 14 shows the variations of heat transfer coefficient at the high-pressure and low-pressure side, respectively. It is observed that in the four-stage RCTTHE the heat transfer coefficient of high-pressure side is higher than that of the low-pressure side, which means the thermal resistance occurs mainly on the low-pressure side. Furthermore, the heat transfer coefficients of RCTTHE-3 and RCTTHE-4 are much smaller than that of RCTTHE-1 and RCTTHE-2. The decrease of the heat transfer coefficients will seriously affect the heat transfer effectiveness, thereby causing the degradation of the hybrid cryocooler performance. Especially for RCTTHE-4, its effectiveness directly affects the cooling temperature and cooling capacity of the hybrid cryocooler as discussed in Section 2.2.

Fig. 15 shows that the variations of heat transfer coefficient on the high-pressure side in the RCTTHE-3 and RCTTHE-4 with different high-pressures. It is observed that increasing the high-pressure can significantly improve the heat transfer coefficient of the high-pressure side. Compared with RCTTHE-1, RCTTHE-2 and RCTTHE-3, the effect of the high-pressure on the heat transfer coefficient in RCTTHE-4 is more pronounced.

Therefore, reducing the geometric size including cross-sectional area and spiral diameter can increase the heat transfer coefficient of the RCTTHE, thereby improving the heat transfer effectiveness. For RCTTHE-4 with the lower heat transfer coefficient, the high-pressure should be increased to improve the heat transfer coefficient of the high-pressure side. Besides, improving the heat transfer coefficient rather than heat transfer area is a better approach to improve heat exchanger effectiveness when the effectiveness is higher than 97 %.

4.2. Pressure drop

Combining mass flow rate with Eq. (28), ΔP_a is determined by:

$$\Delta P_a = \frac{8fL\dot{m}^2}{\pi^2\rho(D_3 - D_2)^3(D_3 + D_2)^2} \tag{37}$$

As shown in Eq. (38), the pressure drop is inversely proportional to density while proportional to the square of mass flow rate. Fig. 16 shows variations of the pressure drops at the low-pressure side with the mass flow rate in different inner diameters of the outer tube. It is observed that the pressure drop of each stage RCTTHE increase with the increase of the mass flow rate. Furthermore, the pressure drop of the RCTTHE-1 increase sharply as D_3 decreases. It is also found that the pressure drops mainly occurs in RCTTHE-1, for which the reason is that in the range of 100–300 K, the density of He-4 in RCTTHE-1 is much lower than that in RCTTHE-2, RCTTHE-3 or RCTTHE-4, which results in the increase of velocity in RCTTHE-1. Thus, the pressure drop in RCTTHE-1 at the low-pressure side should remain small enough to achieve the lower evaporation pressure after throttling.

Decreasing the mass flow and increasing D_3 at the low-pressure side can decrease the pressure drop of the RCTTHE. A trade-off between the pressure drop and the heat transfer effectiveness of the 1.8 K hybrid cryocooler should be made to meet the requirement that a pressure drop of 2.03 kPa and heat transfer effectiveness higher than 97 % can be achieved at the same time.

5. Experimental verification

5.1. Experimental setup

For practical applications, the high effectiveness and low pressure drop at low-pressure side are required for the RCTTHE system while the compactness is remained. Therefore, the length of RCTTHE should be as short as possible, and the spiral diameters should be as small as possible according to the JT cycle geometry. In addition, with the maximum pressure drop at low-pressure side kept lower than 2.03 kPa, the inner diameter of outer tube is reduced to achieve a higher heat transfer coefficient. And then the optimal dimensional parameters of the four-stage RCTTHEs are acquired according to the relevant calculation discussed in Section 4. The dimensional parameters of the four-stage RCTTHEs are listed in Table.1.

Based on the above theoretical analyses and optimization results, the actual RCTTHE system is developed, as shown in Fig. 17. It is coupled to the 1.8 K hybrid cryocooler for the experimental verifications. Fig. 18 shows the actual experimental setup of the 1.8 K hybrid cryocooler. Eight thermometers are used to measure the temperatures of 1st PHEX, 2nd PHEX and 3rd PHEX (Points 3, 5 and 7 in Figs. 1 and 2) of the four-stage Stirling-type pulse tube cryocooler subsystem, and the temperature of the evaporator (Point 10 in Figs. 1 and 2), the hot end temperature of RCTTHE-4 (Point 11 in Figs. 1 and 2), the hot end outlet temperature of RCTTHE-3 (Point 12 in Figs. 1 and 2), the hot end outlet temperature of RCTTHE-2 (Point 13 in Figs. 1 and 2) and helium temperature before throttling (Point 8 in Figs. 1 and 2) of JT cryocooler subsystem, respectively. The details of the sensors are listed in Table 2.

5.2. Experimental validation of model

As shown in Table 1, in terms of RCTTHE effectiveness, the simulation and experimental results are in good agreement. The effectiveness of the four-stage RCTTHEs are higher than 97.1 %.

Fig. 19 shows the experimental results of the 1.8 K hybrid cryocooler based on the optimized four-stage RCTTHE. Both cooling temperature and mass flow rate decrease with the decrease of the high pressure before throttling. The hybrid cryocooler can obtain a no-load temperature of 1.8 K with the mass flow rate of 0.32 mg/s, of which the high pressure is 0.32 MPa.

Fig. 20 shows the simulated and measured ΔP with different mass flow rates. The simulated pressure drop is in good agreement with the measured value. The pressure drop of the RCTTHE system increases with the increasing mass flow rate, and the maximum difference between simulations and experimental results does not exceed 0.32 kPa with the mass flow rate from 0.5 to 3 mg/s.

Fig. 21 shows the temperature curves obtained from simulations and experiments. It is observed that the temperature difference between the two curves gradually increases along the length of the RCTTHE, and eventually reaches the maximum value at the cold end of the RCTTHE. It means that the heat transfer coefficients on both sides decrease with the decrease of temperature as shown in Figs. 11 and 12.

In summary, good agreements are found between theoretical and experimental results, which means the method described in this paper is a good way to design and optimize the RCTTHE for the 1.8 K hybrid cryocooler. Furthermore, flow and heat transfer mechanisms of RCTTHE system can be analyzed to help understand the hybrid cryocooler under different working conditions.

6. Conclusions

This paper conducts theoretical analyses and experimental verifications of a four-stage RCTTHE operating in the range of 4–300 K, which is used in a 1.8 K hybrid cryocooler formed by a four-stage Stirling-type pulse tube cryocooler and a JT cooler.

A finite difference model of fluid–structure interaction for the four-stage RCTTHE is developed, and the empirical correlations of flow and heat transfer are employed to solve the involved equations. Several important factors are considered such as the changes in fluid properties, the radiant heat leakage and the effects of secondary flow.

Flow and heat transfer characteristics of the four-stage RCTTHE are investigated in detail. In the RCTTHE-3 and RCTTHE-4, when the heat exchange effectiveness is higher than 97 %, it should be considered to improve the heat exchange efficiency by increasing the heat exchange coefficient. The inner diameters of both inner tube and outer tube should be reduced to improve the heat transfer coefficient. In addition, the pressure drop of the four-stage RCTTHE mainly occurs in RCTTHE-1, and thus the inner diameter of the outer tube should be minimized to decrease the pressure drop at the low-pressure side in RCTTHE-1.

An improved four-stage RCTTHE system is designed and then integrated into the hybrid cryocooler. Experiments are conducted to verify the theoretical analyses and the results show a good agreement between simulations and experiments. With the optimized four-stage RCTTHE which has a considerably low total pressure drop at low-pressure side of 518 Pa and the heat exchange effectiveness higher than 97.1 %, the developed hybrid cryocooler can obtain a no-load temperature of 1.8 K with a mass flow rate of 1 mg/s and a high pressure of 0.32 MPa.

CRediT authorship contribution statement

Bangjian Zhao: Methodology, Investigation, Data curation, Writing – original draft. **Tao Zhang:** Investigation. **Jun Tan:** Investigation. **Yongjiang Zhao:** Investigation. **Renjun Xue:** Investigation. **Han Tan:** Investigation. **Shiguang Wu:** Investigation. **Yujia Zhai:** Investigation. **Haizheng Dang:** Conceptualization, Methodology, Supervision, Writing – original draft, Writing – review & editing.

Declaration of Competing Interest

The authors declare that they have no known competing financial interests or personal relationships that could have appeared to influence the work reported in this paper.

Acknowledgements

This work is supported by the National Natural Science Foundation of China(Grant No. 52076210) , Shanghai Municipal Science and Technology Major Project(Grant No. 2019SHZDZX01) and Shanghai Municipality (Nos. 18511110100, 19511106800, 2019-jmrh2-kj2 and 2021-cyxt2-kj09).

References

[1] Ross Jr RG. Space coolers: a 50-year quest for long life cryogenic cooling in space. In: Timmerhaus KD, Reed RP, editors. Cryogenic engineering: fifty years of progress. New York: Springer Publishers; 2006. p. 225–284.

[2] Ross Jr RG, Boyle RF. An overview of NASA space cryocooler programs-2006. In: Miller SD, Ross Jr RG, editors. Proceedings of the 14th International Cryocooler Conference. Annapolis: International Cryocooler Conference,2007,14:1–10.
[3] Narasaki K, Tsunematsu S, Ootsuka K, Watanabe N, Matsumoto T, Murakami H, et al. Development of 1 K-class mechanical cooler for SPICA. Cryogenics 2004;44 (6-8):375–81.
[4] Sato Y, Sawada K, Shinozaki K, Sugita H, Mitsuda K, Yamasaki NY, et al. Development of 1K-class Joule-Thomson cryocooler for next-generation astronomical mission. Cryogenics 2016;74:47–54.
[5] Raab J, Tward E. Northrop Grumman Aerospace Systems cryocooler overview. Cryogenics 2010;50(9):572–81.
[6] Petach M, Michaelian M, Nguyen T. Modifications to the MIRI cryocooler design to provide significant lift in the 2 K to 4 K range. IOP Conference Ser Mate Sci and Eng 2020;755(1):012018. https://doi.org/10.1088/1757-899X/755/1/012018.
[7] Kotsubo V, Ullom JN, Nam SW. Compact 1.7 K Cryocooler for Superconducting Nanowire Single-Photon Detectors. Cryocoolers 2018;20:295–304.
[8] Crook M, Bradshaw T, Gilley G, et al. Development of a 2 K Joule-Thomson closed-cycle cryocooler. Cryocoolers 2016;19:9–18.
[9] Zhang T, Dang HZ. Investigations on a 1 K hybrid cryocooler composed of a four-stage Stirling-type pulse tube cryocooler and a Joule-Thomson cooler. Part A: Theoretical analyses and modeling. Cryogenics 2021;116:103282.
[10] Dang H, Tan H, Zhang T, Zha R, Tan J, Zhao Y, et al. A 1–2 K Cryogenic System with Light Weight, Long Life, Low Vibration, Low EMI and Flexible Cooling Capacity for the Superconducting Nanowire Single-Photon Detector. IEEE Trans Appl Supercond 2021;31(5):1–5.
[11] Dang HZ, Zhang T, Zhao BJ, et al. Investigations on a 1 K hybrid cryocooler composed of a four-stage Stirling-type pulse tube cryocooler and a Joule-Thomson cooler. Part B: Experimental verifications Cryogenics 2022;123:103452.
[12] Huang YH, Chen GB. A practical vapor pressure equation for helium-3 from 0.01 K to the critical point. Cryogenics 2006;46(12):833–9.
[13] Dang HZ, Zhang T, Zhao BJ, et al. A hybrid cryocooler achieving 1.8 K with He-4 as the only working medium and its application verification (in Chinese). Chin Sci Bull 2022;67:896–905.
[14] Popov D, Fikiin K, Stankov B, Alvarez G, Youbi-Idrissi M, Damas A, et al. Cryogenic heat exchangers for process cooling and renewable energy storage: A review. Appl Therm Eng 2019;153:275–90.
[15] Nellis GF. A heat exchanger model that includes axial conduction, parasitic heat loads, and property variations. Cryogenics 2003;43(9):523–38.
[16] Pacio JC, Dorao CA. A review on heat exchanger thermal hydraulic models for cryogenic applications. Cryogenics 2011;51(7):366–79.
[17] Maytal BZ, Miniature Joule-Thomson Cryocooling: Principles and Practice. Berlin: Springer; 2013.
[18] Rohsenow WM, Hartnett JP, Cho YI. Handbook of heat transfer. New York: McGraw-Hill; 1998.
[19] Nellis G, Klein S. Heat transfer. Cambridge university press; 2008.
[20] Idelchik I E. Handbook of hydraulic resistance, 4th revised and augmented edition. Begel House Inc.: Connecticut: 2008.